HTML ABSTRACT + LINKS

Micromachined force sensors for the study of cell mechanics

Shengyuan Yang and Taher Saif[a)]
Department of Mechanical and Industrial Engineering, University of Illinois at Urbana-Champaign, Urbana, Illinois 61801

(Received 19 August 2004; accepted 21 December 2004; published online 16 March 2005)

A technique using micromachined mechanical force sensors to measure the force response of living cells is introduced. The force sensors consist of a probe and flexible beams. The probe is used to indent and stretch the cells, and the flexible beams are used to measure the cell force response. The stiffness of the sensors is designed at several nanonewtons per micrometer, but can be varied over a wide range. The sensors are fabricated by the SCREAM process. The deformation of the cells and the deflection of flexible beams are measured by an optical microscope coupled with a charge-coupled device camera. Experimental demonstrations show the feasibility, simplicity, and versatility of this technique. It addresses several disadvantages of existing related techniques, and is complementary to many of them. We expect that this new technique will attract significant attention and be employed much more in the study of cell mechanics. © *2005 American Institute of Physics.* [DOI: 10.1063/1.1863792]

I. INTRODUCTION

Increasing experimental evidence shows that a living cell senses mechanical stimuli and responds with biological changes, which in turn may alter cell internal structure and hence its mechanical behavior.[1–11] Uncovering the mechanical response of living cells is, therefore, important from views of traditional materials science and biological science. The techniques developed for measuring the mechanical response[12,13] of living cells include: centrifugation,[14] shear flow,[15] substrate deformation,[16] substrate composition,[17] flexible substrata,[18] embedded particle tracking,[19] multiple-particle-tracking microrheology,[20] magnetic twisting cytometry,[1] magnetic bead microrheometry,[21] micropatterned substrates,[22] micropipette aspiration,[23] optical traps,[24] optical stretcher,[25] magnetic traps,[26] biomembrane force probe,[27] cell poker,[28] atomic force microscopy (AFM),[29] surface force apparatus,[30] glass needles,[31] shear on single cells,[32] microplates,[33] and tensile tester,[34] with the first four dedicated to cell population studies and the rest focused on single cell and/or single biomolecule studies.

The description of the above techniques and a comparison between them are beyond the scope of this article. Interested readers are referred to the reviews in Refs. 9, 12, and 13. Although these techniques have revealed significant insight on mechanical response of single cells and cell populations, they have limitations. First, they only measure certain types or small ranges of cell deformation and force response, or mechanical response of cells at certain states. For example, the substrate-related techniques only account for the traction force between the cells and substrate; magnetic bead-related techniques, optical traps, and AFM only induce small cell deformation and measure small cell force response; micropipette deforms cells by suction and hence cannot measure the cell indentation mechanical response; microplates and tensile tester only measure suspended cells. Second, the techniques, such as micropipette aspiration, cell poker, AFM, glass needles, microplates, and tensile tester, which measure cell stretch or compression force response, can only measure one component of the force response vector (which normally has three) except AFM, which can measure two (although the measurement of two-component cell force response by AFM has not been reported), and it is difficult to build a system that can measure three force components based on these techniques. Note that a recent article introduces a 3D magnetic twisting device that allows application of a torque to magnetic beads about any chosen axis, and the cell mechanical response can be quantified about this axis.[35] Third, it is difficult to make changes on the measurement systems based on these techniques to adapt to certain measurement applications or working environments. For example, it is difficult to use commercial AFMs with scanning electron microscopes (SEMs) to visualize the structural change of a cell when the cell is stretched or indented by the AFM tip. Fourth, the sensing and control systems for some of the existing techniques are complicated. For example, in magnetic twisting cytometry, complicated hardware is needed to generate and control the required magnet fields. The complexity of commercial AFMs is obvious because of their high-performance optical sensing and feedback electric systems.

In this article, we present a new technique that addresses or improves upon the above disadvantages. In this technique, micromachined mechanical force sensors are used to manipulate cells and measure their force response. The force sensors consist of a probe and some flexible beams. The probe is used to indent or stretch the cells, and the flexible beams to sense the cell force response. Standard optical microscope system is used to record the deformations of the cells and the deflections of the flexible beams. The cell force

[a)]Electronic mail: saif@uiuc.edu

 © 2005 American Institute of Physics

Downloaded 23 Jul 2006 to 130.126.176.129. Redistribution subject to AIP license or copyright, see http://rsi.aip.org/rsi/copyright.jsp

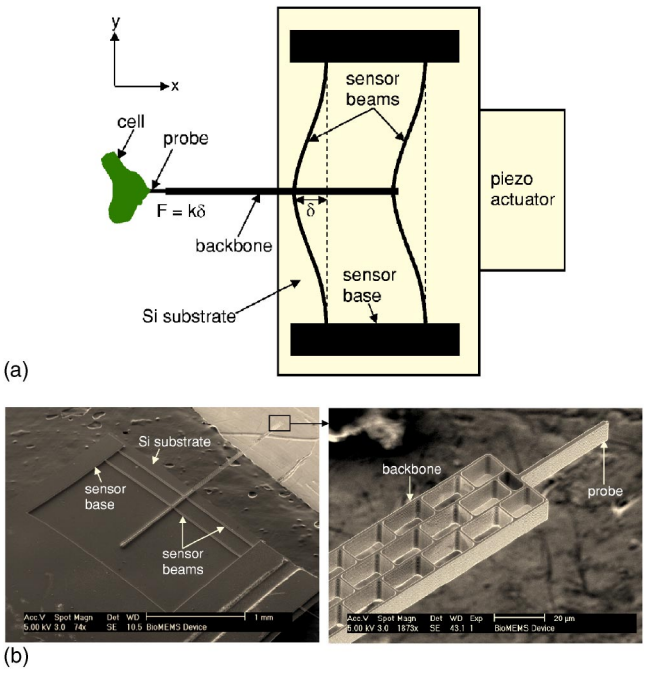

FIG. 1. (Color online) Schematic (a) and SEM image (b) of a mechanical force sensor.

response is simply obtained by multiplying the stiffness of the sensors by the sensor deflections. Compared to the existing techniques, it is simpler and more versatile and offers more flexibility for a wide range of cellular exploration. Preliminary experimental results show the feasibility and the advantages of this technique.

II. MATERIALS AND METHODS

A. Force sensor

The schematic and SEM image of a force sensor are shown in Figs. 1(a) and 1(b), respectively. In this sensor, two parallel flexible beams with fixed–fixed boundary conditions serve as the sensor beams. The probe is connected to the sensor beams through a backbone attached to the midpoint of the sensor beams. The chip, on which the sensor is fabricated, is driven by a piezo actuator held by an $x-y-z-\theta_x-\theta_y-\theta_z$ stage. The actuator moves the chip and hence the probe in the x direction to indent or stretch a cell. The stiffness of the sensor in the x direction is much smaller than those in the y and z directions due to high aspect ratio (depth-to-thickness ratio) of the beams and their geometry. Thus, only the deflection of the sensor beams and hence the cell force response in the x direction is measured. The sensor is made of single-crystal silicon (Si) with a Young's modulus $E=170$ GPa (the beams are aligned in the [110] direction of single-crystal Si). The length of each sensor beam is $L=1.96$mm. The cross section of the beam is rectangular, with depth (the dimension perpendicular to the paper) $b=10.5$ μm and thickness (the dimension parallel to the paper) $h=0.77$ μm. The stiffness of the sensor (in the x direction) is estimated as $k=3.4$ nN/μm, by

$$k = \frac{384EI}{L^3}, \tag{1}$$

where

$$I = \tfrac{1}{12}bh^3 \tag{2}$$

is the moment of inertia of the beam. The cell force response is then obtained from

$$F = k\delta, \tag{3}$$

with δ being the deflection of the sensor beams. The exact value of this sensor stiffness may not be so critical in many cell experiments if one is interested in the qualitative characteristics of cell force response when the sensor stiffness behaves as a scale factor, as in the case of most AFM measurements. The sensor stiffness can also be calibrated independently against another spring with known spring constant. The method of calibration is described in the Appendix, where the stiffness of a sensor is calibrated and compared with that estimated from Eq. (1), and they match closely.

The SCREAM process[36] was used to fabricate the sensor. The process starts with a single-crystal Si wafer (Silicon Quest International). The fabrication steps are as follows (Fig. 2): (a) Grow an oxide (SiO_2) layer ($\sim$1 μm thick) on the surface of the Si wafer by thermal oxidation; (b) Pattern the sensor to the oxide surface by photolithography; (c) Anisotropically etch the oxide layer by reactive ion etching (RIE); (d) Anisotropically etch the Si substrate to the desired depth ($\sim$20 μm) by inductively coupled plasma (ICP); (e) Remove the photoresist (PR) layer by oxygen plasma etching; (f) Thermally oxidize the wafer again to put a protecting oxide layer ($\sim$0.15 μm thick) on the Si surface; (g) Anisotropically remove the oxide layer on the floor of the patterned trench by RIE (this step reduces the thickness of the top oxide layer as well); (h) Anisotropically etch down the exposed Si again for an additional depth ($\sim$10 μm) by ICP; (i) Isotropically etch the exposed Si to release the beams by ICP; (j) Remove all the oxide by wet hydrofluoride acid etching. Thus, the entire sensor is made of pure single-crystal Si. During the thermal oxidation, Si is consumed to form SiO_2. Hence, the longer the oxidation time, the thinner is the remaining Si, and then the softer is the sensor. Thus, the duration of oxidation allows one to achieve various stiffness of the sensor from the same initial design. Note that the last step in the SCREAM process is metallization, which is avoided here.

B. Experimental system

The experimental system using the sensor to measure the cell force response is shown in Fig. 3. Here, the sensor is fixed to a holder which is mounted on an $x-y-z$ piezo stage with 1 nm resolution, and the piezo stage is in turn mounted on an $x-y-z$ mechanical stage with 1 μm resolution. The mechanical stage is mounted on a tilt and rotation platform. An inverted optical microscope (Olympus CK40) with an objective of 10$\times$ is used to monitor the deformation of the cell and the displacement of the sensor probe. Through an adaptor of 2.5$\times$, images are recorded using a cooled CCD

Downloaded 23 Jul 2006 to 130.126.176.129. Redistribution subject to AIP license or copyright, see http://rsi.aip.org/rsi/copyright.jsp

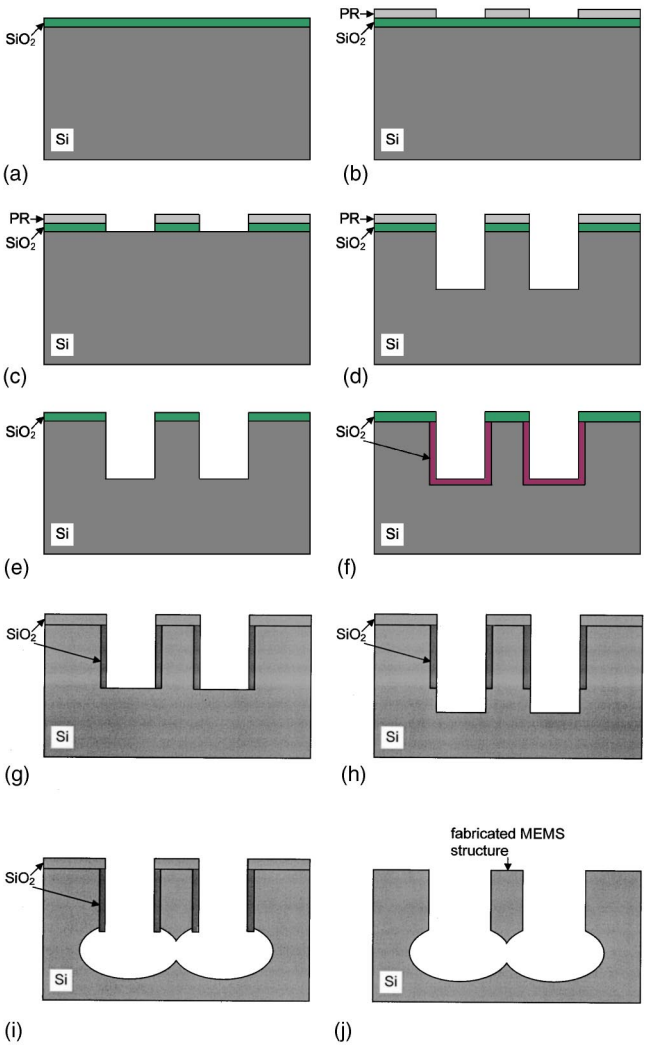

FIG. 2. (Color online) SCREAM process used to fabricate the sensor.

camera (Olympus MagnaFire S99806) with an imaging pixel size of 1280×1024 and its image acquisition software. By measuring structures with known sizes, the resolution of the images was determined as 0.27 μm per pixel. Thus, the dimensional measurement accuracy (error) is $\Delta=0.27\ \mu\mathrm{m}/2 \approx 0.14\ \mu$m. The force resolution of the system is estimated as $k\Delta \approx 0.5$ nN [Eq. (3)]. The cells are cultured in a 35 mm dish, and the sensor is immersed in the culture medium for cell force response measurement. The sensor plane is inclined by 5 deg with respect to the bottom of the culture dish to ensure that the contacting tip of the sensor probe has the lowest elevation.

The deformation of a cell in the x direction is positive when the cell is elongated, and negative when shortened (indented); the deformation in the y direction is defined positive upward in the images. The cell force response is positive when the probe–cell interaction is in tensile state. The cell deformation is given by the displacement of the contact point between the cell and the probe, and the sensor deflection is measured from the relative displacements between the probe and the sensor base. In the experimental results shown below, the cell deformations and force response are measured with respect to the initial state where the probe contacts the

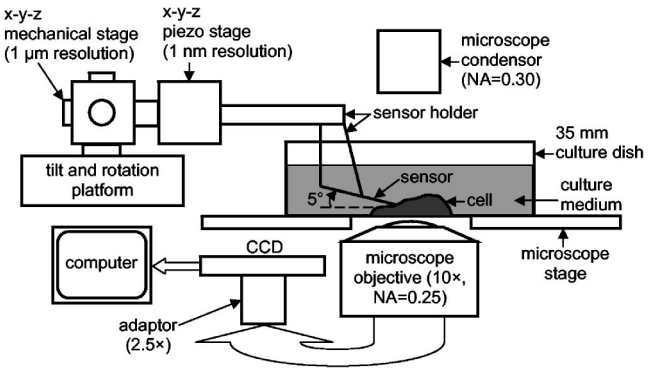

FIG. 3. Experimental system and the sensor to measure the cell force response.

cell. For the experimental results shown in this article, each deformation increment (decrement) was accomplished in 1 s by manually increasing (decreasing) the voltage for the piezo stage. The cell deformation and force response were recorded (by capturing the corresponding phase contrast image) 15 s after each deformation increment (decrement), and the exposure time for capturing the image was less than 1 s. The time delay between two consecutive deformation increments (decrements) was kept at 50 s unless otherwise stated.

To study cell stretch force response, the sensor probe was also functionalized by coating with fibronectin by incubating the sensor in 50 $\mu\mathrm{g}\cdot\mathrm{ml}^{-1}$ fibronectin (BD Biosciences) solution at room temperature for 6 h. It was then taken out for drying at room temperature for 6 h before it was immersed into the culture medium and brought in contact with a cell for 20 min. The cell forms adhesion sites with the probe most likely by integrin activation.[37] The sites are connected to the cytoskeletal structure and thus offer the probe a localized handle to the cytoskeleton.

The cells tested in this article were cultured from CV-1 (ATCC), a monkey kidney fibroblast (MKF) cell line. They were cultured in a medium with 90% DMEM (ATCC) and 10% FBS (ATCC) in an environment with 37 °C temperature, 5% CO_2, and were plated for 24–48 h before the experiments. The cell force response measurement was conducted in air at room temperature.

III. RESULTS

A. Cell morphology change due to small mechanical disturbance

The technique introduced above was used to study the morphological change of living cells (attached to the bottom of a dish) due to a mechanical disturbance. In this case, the sensor probe was brought in contact with the cells to laterally indent them by a small amount ($\sim 2\ \mu$m). The change of shape of the cells was recorded for a period of time with the sensor base fixed. Figure 4(a) shows the cell right after the indentation, while Fig. 4(b) shows the state 72 min after Fig. 4(a). We see the obvious shape change of the cell, and the mechanical indentation was reduced, as if the cell was staying away from the probe. Figures 4(c)–4(e) show the results for a different cell. Here, the cell was dividing and was at its

Downloaded 23 Jul 2006 to 130.126.176.129. Redistribution subject to AIP license or copyright, see http://rsi.aip.org/rsi/copyright.jsp

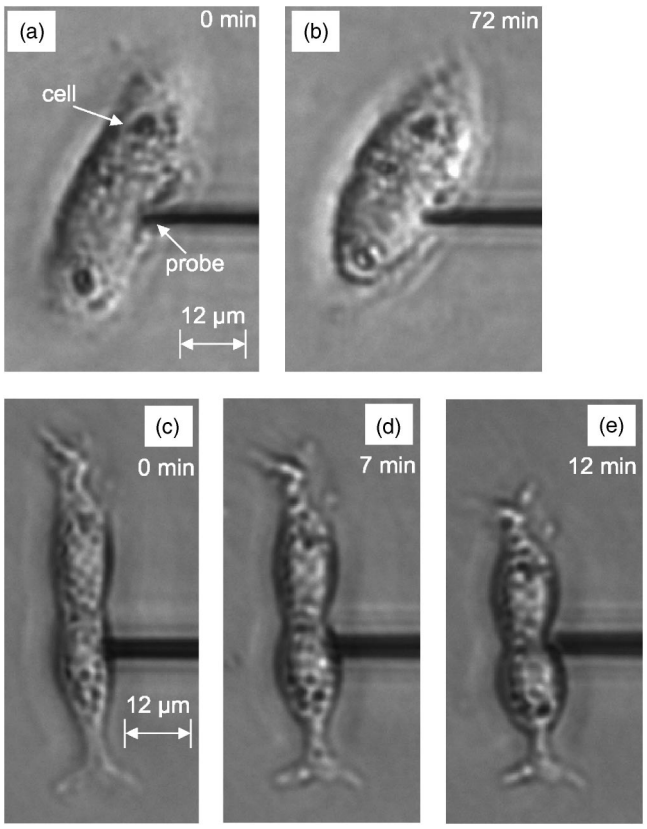

FIG. 4. Morphological changes of two cells due to mechanical disturbance of the sensor probe. (a) Right after the probe indented a monkey kidney fibroblast (MKF); and (b) 72 min after (a). (c) Right after the probe indented an MKF; (d) and (e) seven min and 12 min after (c), respectively.

telophase. Figure 4(c) shows the state right after the probe indented the cell, and Figs. 4(d) and 4(e) are the states 7 min and 12 min after Fig. 4(c), respectively.

B. One-component force sensing

The technique was used to study the force response of living cells subject to large lateral indentation. In this case, the cells were laterally indented by a small amount (as above) for 20 min. If cell shape change (as observed in Fig. 4) was not observed, further indentation was conducted and the corresponding cell force response was measured. Figure 5 shows the results for a cell under indentation. Figure 5(a) shows the force response. Figures 5(b)–5(f) are representative phase contrast images. In Fig. 5(a), the slope within Figs. 5(b) and 5(c) is larger than that within Figs. 5(c) and 5(d), which may be attributed to partial breaking of the attachment of the cell with the substrate. After the linear force response stage, the cell yielded, i.e., from Figs. 5(d)–5(f) the cell indentation increased without corresponding increase in force response.

A functionalized sensor was used to study cell stretch force response. In this case, the probe of the sensor was brought in contact with the cells for 20 min to form the adhesion site. Figure 6 shows the results for an elongated cell. Here, the focal adhesion connection formed between the probe and the cell is relatively small compared to the cell size, and the induced stretch deformation of the cell is local. Figure 6(a) is the stretch force response. Figures 6(b)–6(f)

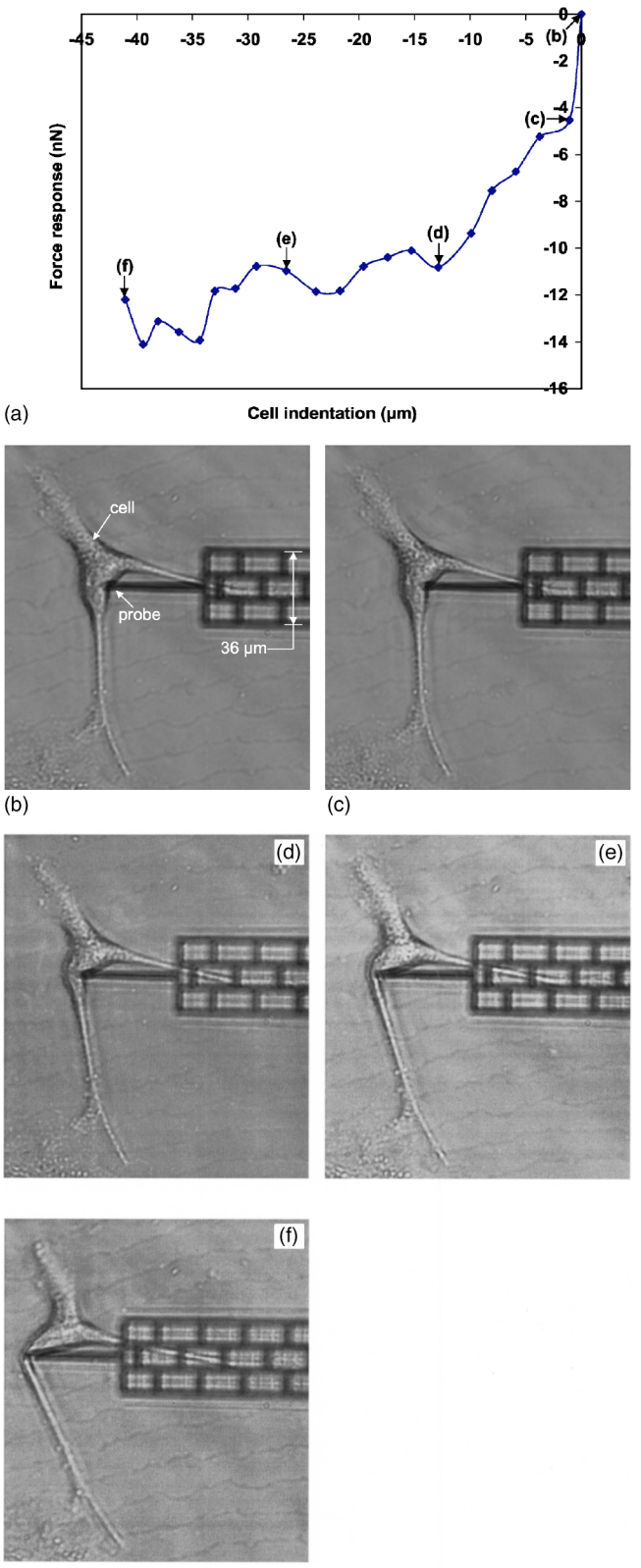

FIG. 5. Force response of an MKF due to large lateral indentation. (a) Force response. (b)–(f) Representative phase contrast images.

are representative phase contrast images. From Figs. 6(b)–6(d) the cell force response is small and does not show a significant trend, possibly because the cytoskeleton has not yet been brought under tension. From Fig. 6(d)–6(f) the cell force response shows a significant linear trend.

Downloaded 23 Jul 2006 to 130.126.176.129. Redistribution subject to AIP license or copyright, see http://rsi.aip.org/rsi/copyright.jsp

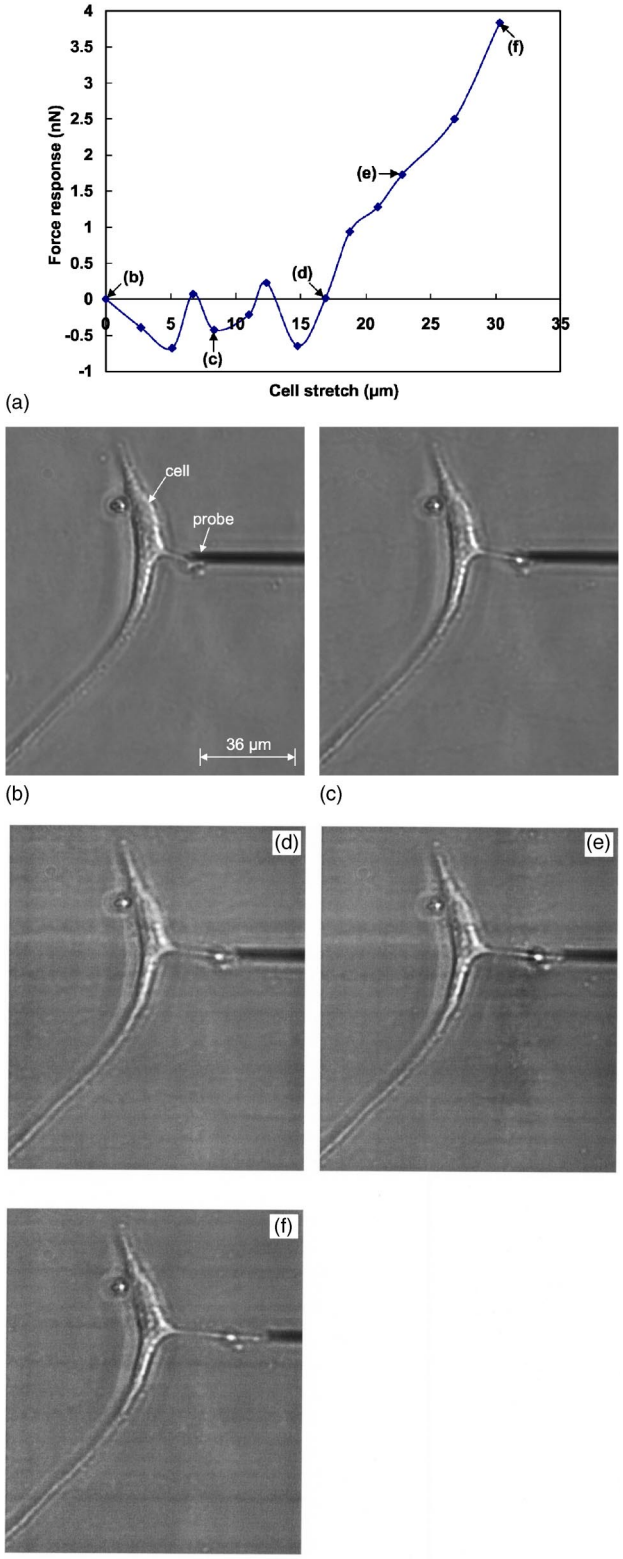

FIG. 6. Stretch force response of an MKF with a small adhesion site with the sensor probe. (a) Force response. (b)–(f) Representative phase contrast images.

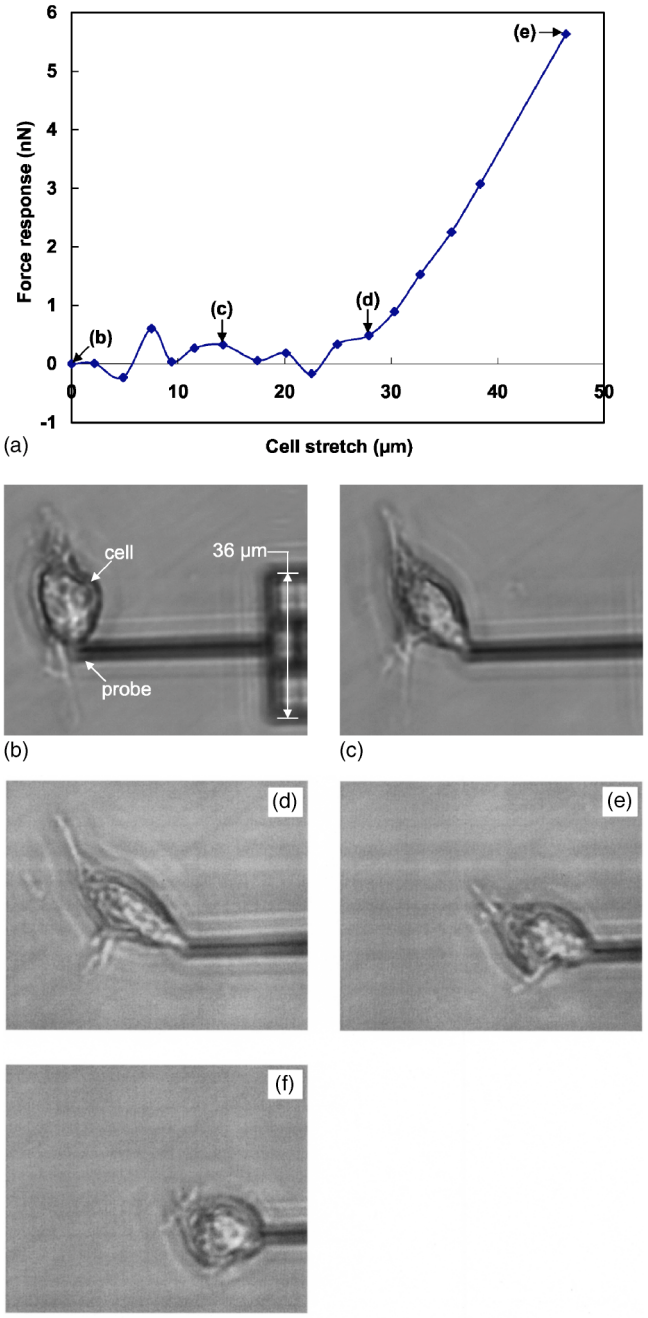

FIG. 7. Stretch force response of an MKF with a large adhesion site with the sensor probe. (a) Force response. (b)–(f) Representative phase contrast images.

In the experiment for Fig. 7, a relatively large adhesion site was formed between the probe and the cell, and the induced stretch deformation of the cell is global, i.e., the entire cell deforms. Figure 7(a) is the stretch force response. Figures 7(b)–7(f) are representative phase contrast images. The force response is similar to Fig. 6. From Figs. 7(b)–7(d) the cell force response is small and does not show a significant trend, and the cell underwent alignment due to the stretch. From Figs. 7(d) and 7(e), the cell force response is linear, and the cell underwent significant migration. Figure 7(f) is the image taken 85 s after Fig. 7(e).

C. Two-component force sensing

Although a cell may be deformed in one direction, it may generate force response in orthogonal directions. One needs a sensor that measures the force response in multidi-

Downloaded 23 Jul 2006 to 130.126.176.129. Redistribution subject to AIP license or copyright, see http://rsi.aip.org/rsi/copyright.jsp

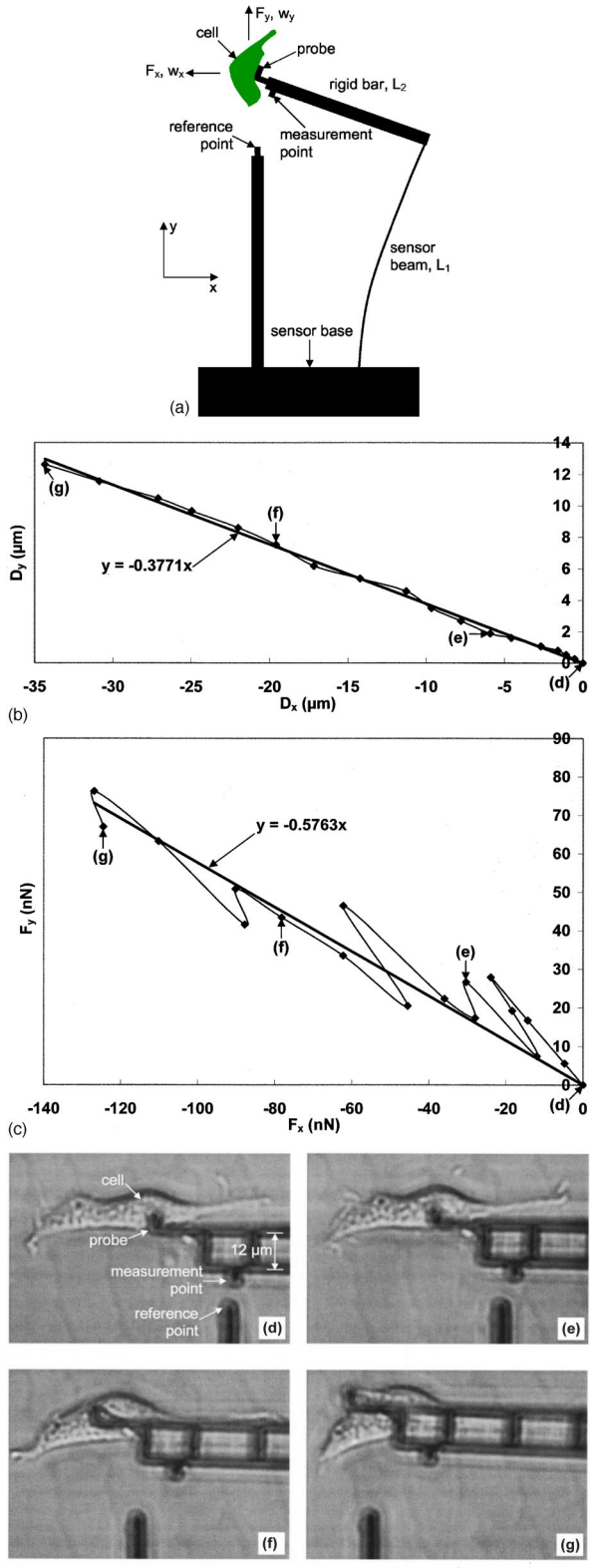

FIG. 8. (Color online) (a) Two-component force sensor. (b) Cell deformation vector. (c) Force response vector. (d)–(g) Representative phase contrast images.

mension as well. Such information may provide insight on the mechanobiological behavior of the cell. In the following we introduce such a force sensor.

Figure 8(a) shows the schematic of the two-component force sensor. Here, the sensor beam deforms due to both force components F_x and F_y, and the probe tip displaces by w_x and w_y with respect to the sensor base, in the x and y directions, respectively. The force components can be obtained from

$$\begin{bmatrix} F_x \\ F_y \end{bmatrix} = \frac{2EI}{L_1^3} \begin{bmatrix} 6 & 3\frac{L_1}{L_2} \\ 3\frac{L_1}{L_2} & 2\left(\frac{L_1}{L_2}\right)^2 \end{bmatrix} \begin{bmatrix} w_x \\ w_y \end{bmatrix}. \tag{4}$$

The cell deformations D_x and D_y are the motion of the probe tip and hence the contact point with the cell with respect to the lab frame of reference. Thus, D_x and D_y are different from w_x and w_y. If the cell does not have any force response, then $w_x = w_y = 0$, but D_x or D_y are nonzero. We demonstrate the applicability of the sensor by measuring the force response of a cell. The sensor geometry is $L_1 = 1$ mm and $L_2 = 0.429$ mm, with a beam cross section of 2.0×13.1 μm. Thus, by Eq. (4), if $w_x = 1$ μm, $w_y = 0.5$ μm, then $F_x = 28.2$ nN, $F_y = 36.9$ nN. Figure 8(b) shows the cell deformation vector (D_x, D_y), and Fig. 8(c) shows the cell force response vector (F_x, F_y), where F_y is defined positive upward [Fig. 8(a)]. Figures 8(d)–8(g) are representative phase contrast images. The deformation vector is almost linear, and the force response vector is roughly linear. But, the slopes for the corresponding linear fits, $y = -0.3771x$ and $y = -0.5763x$, are different, indicating the anisotropy of the mechanical behavior of the cell.

IV. DISCUSSION

The technique presented here, based on micromachined mechanical force sensors, falls into the same category as cell poker, AFM, and glass needles in terms of the basic force sensing principle. But, the above experimental results and the following discussion show the simplicity, versatility, and flexibility of the presented technique, which may not be routinely achieved by the cell poker, AFM, and glass needles, as illustrated by the limitations of the existing techniques given in the Introduction.

The current sensor was designed to measure cell force response due to large stretches and indentations. However, the force resolution ($\sim$0.5 nN) of the sensors demonstrated is too large to be useful in the study of single ligand–receptor force interactions, which can be studied by AFM or optical tweezers. By changing the geometry of the microbeams, the combined spring constant of a sensor can be varied from 10 pN/μm to 1 μN/μm to reach the necessary force sensitivity requirement. According to Eqs. (1) and (2), the stiffness of a force sensor can be reduced (to reach a higher force resolution) by increasing the length or by decreasing the thickness of the sensor beam, both of which have the same cubic dependence ($1/L^3$ and h^3). For a Si beam with dimension $L \times b \times h = 3$ mm $\times 10$ μm $\times 0.5$ μm, we get $k = 0.25$ nN/μm. Doubling the length will decrease the stiffness by about an order of magnitude. But, both increasing the length and reducing the thickness will increase the difficulty of fabrication. The stiffness can also be reduced by serial connection of sensor beams. For example, in the design shown in Fig. 9, two more sets of the sensor beams are

Downloaded 23 Jul 2006 to 130.126.176.129. Redistribution subject to AIP license or copyright, see http://rsi.aip.org/rsi/copyright.jsp

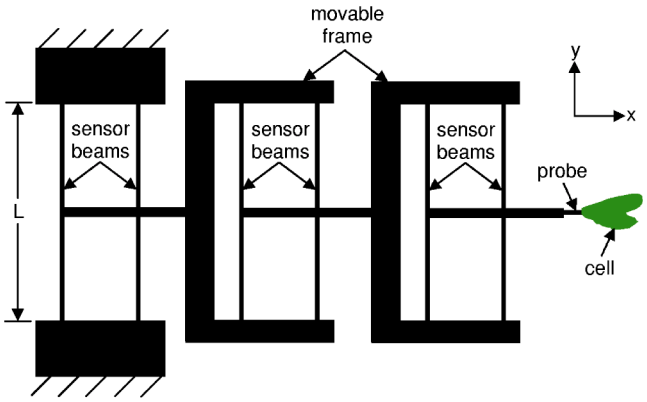

FIG. 9. (Color online) Reducing the stiffness of the force sensor by serially adding the sensor beams.

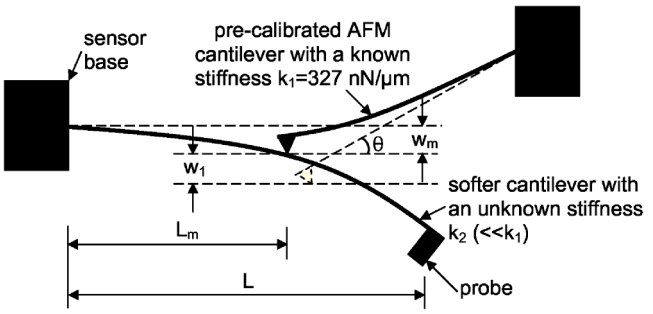

FIG. 10. Calibrating the stiffness of a softer cantilever by a precalibrated AFM cantilever.

serially added to the design of Fig. 1, and the total stiffness of the sensor becomes one-third of that in Fig. 1. Sensors with two sets of serially connected sensor beams (pictures not shown) have been successfully fabricated without significantly increasing the difficulty of fabrication. Therefore, in principle we may reduce the stiffness of the sensor to desired lower values by the combined utilization of the above strategies, i.e., increasing the length, reducing the thickness, and using serial connection of sensor beams. Based on the available versatile microelectromechanical systems (MEMS) fabrication technique, various shapes of the sensor probe can be designed to reach desired contact with cells. The probe can then induce small or large deformation, and the sensor can also measure small or large force response. For example, if a sharp tip is used, the sensor works like an AFM, but probing can be done normal or lateral to the surface of the substrate. In the above experiments, because the increase (decrease) of the voltage for the piezo stage was achieved manually, the rate of the induced cell deformation is slow compared with those of AFM and magnetic twisting cytometry. But, by using a computer-controlled power supply for the piezo stage, together with a high-speed camera, higher rates of deformation comparable to those of AFM can be achieved.

Due to the vertical indentation nature of AFM[29,38–40] and small cell thickness, the allowable cell deformation range is limited and the measured cell mechanical behavior needs careful interpretation due to the influence of the substrate. Using the lateral indentation technique, as shown here, this limitation can be avoided.

In this technique, the cell force response is obtained by multiplying the deflection of the sensor beams by their combined spring constant. Thus, no further calculation or interpretation is needed to measure cell force response. The sensors can be incorporated with laser tweezers and environmental SEMs, and in principle there is no need to change these analytical instruments. The sensors can also be redesigned to orient and adapt to specific new applications. The experimental system is much simpler and more flexible compared to the existing techniques, and no specialized detection and control systems are needed.

There is, however, one limitation about this technique. The microforce sensors have to survive the capillary forces as they are immersed from air to liquid, or emerge from liquid to air. For example, the final step in the fabrication process is the wet etching of SiO_2 on the released sensor beams (Fig. 2). The sensors need to be wet-cleaned by chemical solutions, such as water, acetone, and isopropanol, before they are used to measure the force response of living cells. In functionalizing the sensors, they need to be immersed into the relevant liquid coating medium, such as the fibronectin solution used here. When the sensors are used to measure the force response of living cells, they need to be inundated in the liquid cell culture medium. The capillary forces acting on the sensors during these processes may be large enough to damage the structures of the sensors. Such forces thus pose a limitation on the softness of the sensor beams. However, our experimental experience suggests that the design of the sensor shown in Fig. 1 normally survives the above liquid processes because the fixed–fixed boundary conditions prevent excessive deflections. Moreover, normally it is the taking-out-of-liquid process that breaks the cantilevered sensor beam in Fig. 8(a), and not the putting-into-liquid process, which may be due to the capillary force for putting-into-liquid process being much smaller than that for taking-out-of-liquid.[41] To minimize the possibility of damage due to the capillary forces from the coating medium, one may choose to coat only the probe part of the sensor in the functionalization step.

Additionally, the contact nature between the sensor probe and the cells is complex. The interaction details between the tip of the sensor probe and the cell surface are currently unknown when the sensor probe is brought in contact with a cell. However, since the materials composing the cell are much softer than that of the probe, the contact region will conform with the shape of the probe.

ACKNOWLEDGMENT

This work was supported by National Science Foundation (NSF) Grant ECS 01-18003.

APPENDIX: CALIBRATION OF THE FORCE SENSORS

A commercial AFM (Digital Instruments Dimension 3100) with a precalibrated cantilever may be used to calibrate the stiffness of the force sensors, by measuring the force-deflection relationship of the sensors, for the technique presented in this article. The stiffness of the softest precalibrated commercial AFM cantilever that we could obtain is 327 nN/μm (Veeco Instruments CLFC-NOBO). To demon-

Downloaded 23 Jul 2006 to 130.126.176.129. Redistribution subject to AIP license or copyright, see http://rsi.aip.org/rsi/copyright.jsp

strate the feasibility of this method for calibration of sensor stiffness, and to show how accurate the estimation of sensor stiffness [by Eqs. (1) and (2) based on the measured geometry] could be, another sensor with the same design as that shown in Figs. 1(a) and 1(b) but with a shorter length of 0.962 mm was fabricated, so that the stiffness of the precalibrated cantilever and that of the sensor are close to each other. The cross section of the sensing beam for this sensor has the dimensions $b=10.3$ μm and $h=0.93$ μm. The estimated stiffness is $k=51$ nN/μm. The corresponding value obtained by the calibration is 70 nN/μm. Thus, the error of the estimation is 27% which, in general, is acceptable for absolute force measurement for biological applications. The error of the estimation may arise from the deviation of the cross section of the beams with respect to the idealized rectangular assumption, the nonuniformity of the cross section along the length of the beams, and the measurement error for the beam dimensions.

Softer sensors can also be calibrated by using softer precalibrated cantilevers. Since such soft precalibrated cantilevers are not commercially available, we propose the following approach to develop them. Here, a long cantilever is fabricated from thermally grown SiO_2 on bare Si wafer. It is well known that SiO_2 films have uniform thickness. The stiffness of a cantilever depends on its length as $k \propto 1/L^3$. Alternatively, the stiffness depends on where it is measured. The SiO_2 cantilever will be calibrated at $L_m < L$ (Fig. 10) by the precalibrated AFM cantilever, where L_m is the position on the cantilever at which the force-deflection relationship is measured and L is the total length of the cantilever. Then, the stiffness at the tip is simply $k=k_m(L_m/L)^3$, with k_m being the stiffness at L_m. L_m is chosen such that the estimation of the stiffness of the cantilever at L_m is similar to $k_1 \cos\theta$, i.e., $3EI/L_m^3 \approx k_1 \cos\theta$, with k_1 being the stiffness of the precalibrated AFM cantilever, and θ being the angle between the softer cantilever (to be calibrated) and the AFM cantilever. The reason for this is to reduce the calibration error of the cantilever. Here, k_m is obtained by $k_m=(k_1 w_1 \cos\theta)/w_m$ according to the measured force-deflection relationship at L_m, where $w_1 \cos\theta$ is the deflection of the AFM cantilever and w_m is the deflection of the soft cantilever at L_m. Since the stiffness of the cantilever is inversely proportional to the cube of the cantilever length, this method can be used to establish calibrated cantilevers with stiffness down to two orders of magnitude lower than that of the AFM cantilever. It should be noted, however, that the uniformity of the width of the SiO_2 cantilever depends on the fabrication accuracy. Since the cantilever will be deformed out of plane, the stiffness of the cantilever depends linearly on width. For a wide cantilever, the inaccuracy introduced by the variation of the width along the length is negligible.

[1] N. Wang, J. P. Butler, and D. E. Ingber, Science **260**, 1124 (1993).
[2] D. C. Van-Essen, Nature (London) **385**, 313 (1997).
[3] K.-D. Chen, Y.-S. Li, M. Kim, S. Li, S. Yuan, S. Chien, and J. Y.-J. Shyy, J. Biol. Chem. **274**, 18393 (1999).
[4] N. Q. Balaban *et al.*, Nat. Cell Biol. **3**, 466 (2001).
[5] G. T. Charras and M. A. Horton, Biophys. J. **82**, 2970 (2002).
[6] D. J. Webb, J. T. Parsons, and A. F. Horwitz, Nat. Cell Biol. **4**, E97 (2002).
[7] J. D. Humphrey, Proc. R. Soc. London, Ser. A **459**, 3 (2003).
[8] D. E. Ingber, J. Cell. Sci. **116**, 1157 (2003).
[9] G. Bao and S. Suresh, Nat. Mater. **2**, 715 (2003).
[10] D. J. Tschumperlin *et al.*, Nature (London) **429**, 83 (2004).
[11] T. M. Suchyna, S. E. Tape, R. E. Koeppe, O. S. Andersen, F. Sachs, and P. A. Gottlieb, Nature (London) **430**, 235 (2004).
[12] Y. F. Missirlis and A. D. Spiliotis, Biomol. Eng. **19**, 287 (2002).
[13] K. J. Van Vliet, G. Bao, and S. Suresh, Acta Mater. **51**, 5881 (2003).
[14] G. C. Easty, D. M. Easty, and E. J. Ambrose, Exp. Cell Res. **19**, 539 (1960).
[15] M. J. Levesque, R. M. Nerem, and E. A. Sprague, Biomaterials **11**, 702 (1990).
[16] A. J. Banes, J. Gilbert, D. Taylor, and O. Monbureau, J. Cell. Sci. **75**, 35 (1985).
[17] C. M. Lo, H. B. Wang, M. Dembo, and Y. L. Wang, Biophys. J. **79**, 144 (2000).
[18] A. K. Harris, P. Wild, and D. Stopak, Science **208**, 177 (1980).
[19] S. Munevar, Y.-L. Wang, and M. Dembo, Biophys. J. **80**, 1744 (2001).
[20] Y. Tseng, T. P. Kole, and D. Wirtz, Biophys. J. **83**, 3162 (2002).
[21] A. R. Bausch, F. Ziemann, A. A. Boulbitch, K. Jacobson, and E. Sackmann, Biophys. J. **75**, 2038 (1998).
[22] J. L. Tan, J. Tien, D. M. Pirone, D. S. Gray, K. Bhadriraju, and C. S. Chen, Proc. Natl. Acad. Sci. U.S.A. **100**, 1484 (2003).
[23] E. Evans, D. Berk, and A. Leung, Biophys. J. **59**, 838 (1991).
[24] J. W. Dai and M. P. Sheetz, Biophys. J. **68**, 988 (1995).
[25] J. Guck, R. Ananthakrishnan, C. C. Cunningham, and J. Kas, J. Phys.: Condens. Matter **14**, 4843 (2002).
[26] C. Haber and D. Wirtz, Rev. Sci. Instrum. **71**, 4561 (2000).
[27] R. Merkel, P. Nassoy, A. Leung, K. Ritchie, and E. Evans, Nature (London) **397**, 50 (1999).
[28] N. O. Petersen, W. B. McConnaughey, and E. L. Elson, Proc. Natl. Acad. Sci. U.S.A. **79**, 5327 (1982).
[29] S. G. Shroff, D. R. Saner, and R. Lal, Am. J. Physiol.: Cell Physiol. **269**, C286 (1995).
[30] C. A. Helm, W. Knoll, and J. N. Israelachvili, Proc. Natl. Acad. Sci. U.S.A. **88**, 8169 (1991).
[31] S. R. Heidemann, S. Kaech, R. E. Buxbaum, and A. Matus, J. Cell. Sci. **145**, 109 (1999).
[32] A. Yamamoto, S. Mishima, N. Maruyama, and M. Sumita, Biomaterials **19**, 871 (1998).
[33] O. Thoumine, A. Ott, O. Cardoso, and J. J. Meister, J. Biochem. Biophys. Methods **39**, 47 (1999).
[34] H. Miyazaki, Y. Hasegawa, and K. Hayashi, J. Biomech. **33**, 97 (2000).
[35] S. Hu, L. Eberhard, J. Chen, J. C. Love, J. P. Butler, J. J. Fredberg, G. M. Whitesides, and N. Wang, Am. J. Physiol.: Cell Physiol. **287**, C1184 (2004).
[36] K. A. Shaw, Z. L. Zhang, and N. C. MacDonald, Sens. Actuators, A **40**, 63 (1994).
[37] B. Alberts, A. Johnson, J. Lewis, M. Raff, K. Roberts, and P. Walter, *Molecular Biology of the Cell* (Garland Science, New York, 2002).
[38] H. Miyazaki and K. Hayashi, Med. Biol. Eng. Comput. **37**, 530 (1999).
[39] A. Touhami, B. Nysten, and Y. F. Dufrene, Langmuir **19**, 4539 (2003).
[40] R. E. Mahaffy, S. Park, E. Gerde, J. Kas, and C. K. Shih, Biophys. J. **86**, 1777 (2004).
[41] T. A. Saif, J. Fluid Mech. **473**, 321 (2002).

Downloaded 23 Jul 2006 to 130.126.176.129. Redistribution subject to AIP license or copyright, see http://rsi.aip.org/rsi/copyright.jsp